Impact of Narrowband Interference on Frequency Synchronization in WLAN-Based OFDM Systems

Brian Leeman*, Davy Pissoort*†, Tim Claeys*
*ESAT-WaveCore, Bruges, KU Leuven, 8200 Bruges, Belgium
†Flanders Make@KU Leuven
{brian.leeman, davy.pissoort, tim.claeys}@kuleuven.be

***Abstract*—Synchronization algorithms in Orthogonal Frequency Division Multiplexing (OFDM) based wireless communication systems are an essential element. Without them, it would be impossible to communicate effectively. However, these algorithms are vulnerable to Narrowband Interference (NBI). This is especially worrisome for Ultra-Reliable Low-Latency Communication (URLLC) systems, meant for mission and safety-critical applications. This paper investigates the effect of a Continuous Wave (CW) NBI on multiple Carrier Frequency Offset (CFO) synchronization algorithms used sequentially in a complete WLAN-based OFDM system. This investigation aims for a holistic analysis of this impact and to analyze the worst case performance which poses the greatest risk to URLLC system reliability. The analysis shows a significantly higher impact on the CFO synchronization estimation performance due to a CW interference compared to that from Additive White Gaussian Noise (AWGN). It also identified a CFO estimator using pilot subcarriers to result in significantly higher maximum frequency synchronization errors than other tested algorithms. This raises concerns that such a CFO estimator might carry too much risk for use in URLLC systems.**

I. Introduction

Synchronization in wireless communication systems tackles the problems of Local Oscillator (LO) phase and frequency errors, sample clock errors and symbol/frame boundary detection/tracking. It is a crucial part of the receiver as it allows for coherent demodulation of the transmitted data. However, synchronization algorithms have the potential to be disrupted by Electromagnetic Disturbances (EMDs), both intentional (i.e. jamming) and unintentional (e.g. other radio systems or unwanted signals leaked from electronics), causing Electromagnetic Interference (EMI). This poses a concern for communication in mission and safety-critical applications such as autonomous systems, Industrial Internet of Things (IIoT), and medical surgical robots, where even brief connectivity loss can cause major safety hazards or economic loss.

These applications use so called Ultra-Reliable Low-Latency Communication (URLLC) technology to accommodate the stringent application requirements. Orthogonal Frequency Division Multiplexing (OFDM) based protocols (e.g. Wi-Fi and 5G) mainly form the basis for URLLC technology, for example IEEE802.11bd and 5G NR V2X for Vehicle-to-Anything (V2X) communication [1]. However, OFDM is known to be vulnerable to Narrowband Interference (NBI). This vulnerability has been explored before in e.g. [2]. Within this context, one problem in particular is of interest: NBI and its effects on synchronization in OFDM systems.

The vulnerability of URLLC to EMI (specifically OFDM synchronization and NBI) and the importance of research in this area was previously explored in [3]. It was shown that an important aspect of URLLC systems is managing risk with regard to unexpected events, one of which is EMI. As such, the idea of risk management for EMI in URLLC systems was proposed in [3]. The first step in this risk management is an in depth risk analysis of OFDM synchronization algorithms under NBI. This paper focuses on a specific part of this risk analysis, namely the influence of NBI on OFDM Carrier Frequency Offset (CFO) synchronization, since remaining CFO errors could cause Inter-Carrier Interference (ICI) in the system, leading to significant system performance degradation.

The effect of NBI on OFDM frequency synchronization was previously explored in [4]. However, (i) that analysis focused solely on ”integer” (with respect to the subcarrier spacing) CFO estimation using preamble symbols, i.e. (ii) no channel propagation was considered, (iii) the system model only considered CFO synchronization errors, and (iv) the analysis focused on average performance of the estimator. Also [5] explored this issue, where an analytic solution for the expected value of a commonly used CFO estimator, using preamble symbols, under NBI was derived. However, (i) that analysis focused solely on average performance of the estimator, (ii) estimators using pilot subcarriers are not considered. Lastly, a part of this work was presented in [6]. This paper further expands on [6] by analyzing the worst-case performance in more depth.

This paper aims for a more holistic analysis which is expected to better represent reality. In order to perform this holistic analysis, the system model used in this paper is based on a Wireless Local-Area Network (WLAN) (i.e. Wi-Fi) system with all possible synchronization errors present. It uses channel propagation and it contains a fully featured receiver system using multiple sequential CFO estimation algorithms, using either preamble symbols or pilot subcarriers. This model is used to perform simulations. Additionally, since risk is the main point of interest, the analysis in this paper goes beyond average estimator performance and includes worst-case performance scenarios.

The paper is organized as follows. In Section II, the system model used for the risk analysis is described, including a detailed description of the CFO estimation algorithms. In Section III, the performed simulations are explained and the risk analysis is performed using the simulation data. Lastly, in Section IV, conclusions are drawn and future work is presented.

978-3-903176-77-5© 2025 IFIP

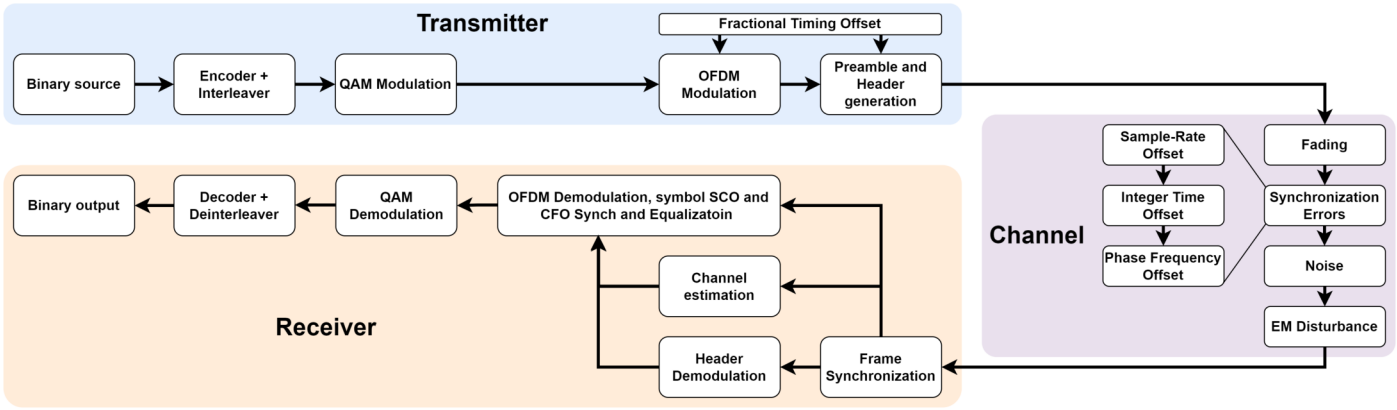

Fig. 1. System model

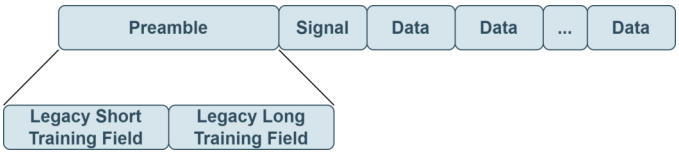

Fig. 2. WLAN-like PHY-frame [3]

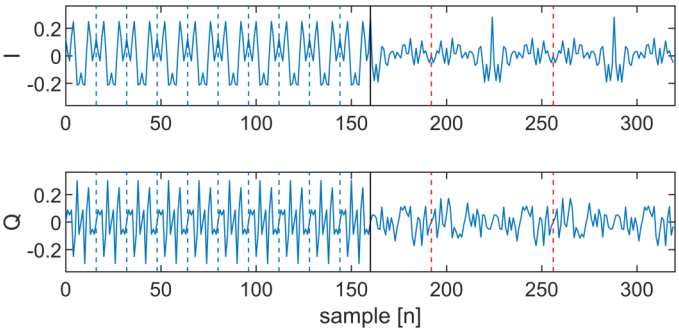

Fig. 3. WLAN-like preamble structure [3]

II. System Model

The WLAN-based system model used for the risk analysis is shown in Fig. 1. The analysis is performed in baseband, and consequently the system model is a baseband model. It consists of three main parts: the transmitter, the channel, and the receiver.

A. Transmitter

The transmitter's objective is creating WLAN-like PHY-frames from the binary input information.

1) Coding, interleaving and OFDM modulation: In order to do this, the bitstream is first encoded using binary convolutional coding and subsequently interleaved according to the WLAN specification [7]. After this, the resulting binary data is modulated using gray-coded m-Quadrature Amplitude Modulation (QAM) and the resulting complex symbols are then OFDM modulated. Additionally, during OFDM modulation, pilot and guardband subcarriers are assigned and a Cyclic-Prefix (CP) is added according to [7].

2) Header and Preamble Generation: The next step of the transmitter is to generate a preamble, identical to the WLAN preamble [7], and a header, the latter of which is also referred to as the signal. The header is a single OFDM symbol and consists of the scrambled bit sequence of a 16-bit integer value presenting the frame length as the number of OFDM symbols in the frame and padding bits, and an 8-bit Cyclic Redundancy Check (CRC) of those scrambled bits. These bits are first Binary Phase Shift Keying (BPSK) modulated and are subsequently OFDM modulated, including the same guardband carriers as before.

Next, the preamble consist of two distinct parts, as shown in Fig. 2: first the Legacy Short Training Field (LSTF) and second the Legacy Long Training Field (LLTF). This structure is shown in more detail in Fig. 3, which shows the preamble in time domain. It is shown that the LSTF, the first half of Fig. 3, is made up of ten repeating sequences each with a length equal to $1/4$th of an OFDM symbol. LLTF is shown in the second half of the figure and is made up of two repeating sequences (OFDM symbols), and is prepended by a CP with twice the length of the normal CP of the system. [7].

3) Assembling the frame: Finally the frame is constructed using the preamble, the header/signal and the OFDM data symbols, specifically in that order. The structure of the WLAN-like PHY-frames is shown in Fig. 2, where the signal field is the header/signal OFDM symbol and the data fields are the OFDM data symbols.

B. Channel

In our study, the channel has the task of adding all the imperfections into the generated PHY-frames. The order in which this happens is as follows.

1) Multipath fading: First, the frames are propagated through a fading channel according to the WLAN TGax channel model [8].

2) Synchronization errors: Next, synchronization errors are added. These include: a Sample-Rate Offset (SRO), an Integer Time Offset (ITO) (i.e. an integer sample delay), a Carrier Phase Offset (CPO) and a CFO. The only exception is the Fractional Timing Offset (FTO) which gets added in the transmitter during OFDM modulation, and preamble and header generation, for efficiency and accuracy reasons in the

simulations. Adding the fractional timing offset during these steps is done using predistortion in the frequency domain, where each OFDM subcarrier gets phase shifted proportional to its subcarrier index. This results in significantly higher computational efficiency and accuracy than any fractional timing offset method in time domain (usually FIR filters) would.

3) Noise and Narrowband Interference: The final steps in the channel are adding Additive White Gaussian Noise (AWGN) and the EMI of interest, a NBI.

The NBI of interest is a Continuous Wave (CW) interference which is modelled according to Equations 1 and 2,

$$\mathrm{CW}[n] = Ae^{i(2\pi f \frac{n}{K} + \varphi)} \tag{1}$$

$$A = \sqrt{P_i} = \sqrt{\frac{P_s}{10^{\mathrm{SIR}/10}}} \tag{2}$$

where $\mathrm{CW}[n]$ is the discrete time (n) CW model. A, f and φ are the CW amplitude, frequency (expressed as a number of subcarriers) and phase, respectively. K is the number of subcarriers in the OFDM system. P_i and P_s are the power of the interference and the power of the OFDM signal, respectively, and SIR is the Signal to Interference Ratio.

C. Receiver

Finally, the receiver has the task to receive and coherently demodulate the imperfect frames. For coherent demodulation, the receiver must perform synchronization procedures, which are by far the most complex part of this system model. This paper focuses solely on CFO. Therefore, perfect synchronization is used for SRO and ITO synchronization. This is achieved by passing the perfect SRO and ITO estimates (known by the simulation model) to the synchronizer and using those for correcting the SRO and ITO synchronization errors. The remainder of the synchronization errors: CPO and FTO, are indirectly corrected for through the channel estimation and equalization operations in the system model. An overview of the receiver's operations and the structure of this section is shown in Fig. 4.

1) Preamble-based Synchronization: The first task of the receiver is performing timing and frequency synchronization using the preamble in the PHY-frames. Timing synchronization is perfect since the synchronizer has been passed the perfect ITO estimates. Frequency synchronization using the preamble is divided into two steps: first, a coarse CFO estimation/correction using the LSTF, and second, a fine CFO estimation/correction using the LLTF. Both methods are based on the Schmidl & Cox algorithm [9].

Coarse CFO Synchronization: Coarse frequency estimation is performed by taking the phase of the autocorrelation of the received signal's LSTF with a delayed copy of itself according to Eqs. 3 and 4, where $\hat{v}_c$ is the coarse frequency estimate expressed in a number of subcarrier spacings, $\angle$ is the argument of a complex number, K is the total number of subcarriers in the OFDM system, L is the length of one LSTF sequence, $p_c \in \mathbb{C}$ is the autocorrelation of the received signal

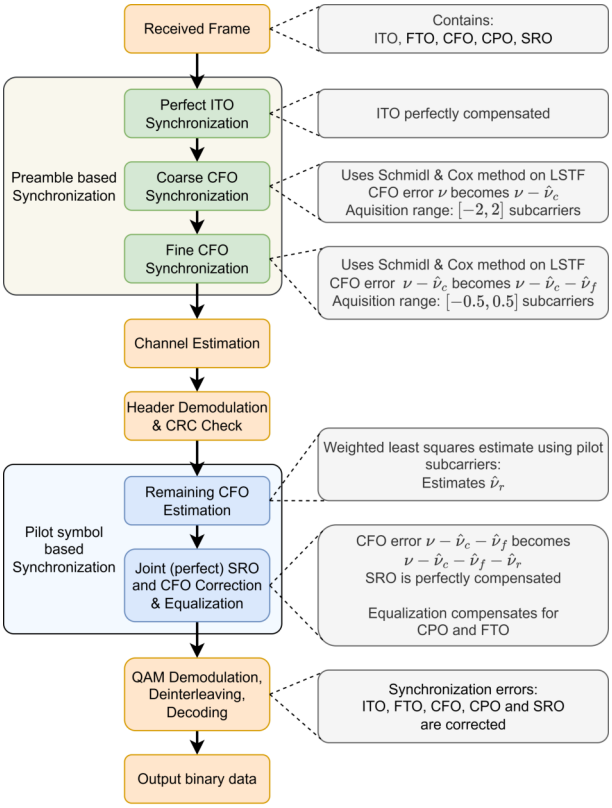

Fig. 4. Receiver structure flowchart

r with the complex conjugate of a delayed copy of itself (with a delay of L), and ϵ_s is the start index of the LSTF in the received signal.

$$\hat{v}_c = \frac{-\angle(p_c)K}{2\pi L} \tag{3}$$

$$p_c = \sum_{n=0}^{9L-1} r[\epsilon_s + n] r^*[\epsilon_s + n + L] \tag{4}$$

After coarse frequency estimation the frequency offset is corrected according to Eq. 5, where $\tilde{r}[n]$ is the corrected signal $\hat{v}$ is the frequency offset the signal is corrected with.

$$\tilde{r}[n] = r[n] e^{i2\pi \frac{-\hat{v}}{K} n} \tag{5}$$

Fine CFO Synchronization: Fine frequency estimation is performed by taking the phase of the correlation of both LLTF sequences in the received signal with each other according to Eqs. 6 and 7, where $\hat{v}_f$ is the fine frequency estimate expressed in a number of subcarrier spacings, ϵ_l is the start index of the first LLTF sequence, $p_f \in \mathbb{C}$ is the correlation of both received LLTF sequences, and K is the total number of subcarriers and consequently the length of a single OFDM symbol/LSTF sequence. This fine frequency estimate is finally corrected, again using Eq. 5.

$$\hat{v}_f = \frac{-\angle(p_f)}{2\pi} \tag{6}$$

$$p_f = \sum_{n=0}^{K-1} r[\epsilon_l + n] r^*[\epsilon_l + n + K] \tag{7}$$

Acquisition Range of Coarse and Fine CFO Estimation Algorithms: One important performance characteristic of these frequency estimation algorithms is their acquisition range. This can easily be calculated by noticing that the phases of p_c and p_f are uniquely defined within $[-\pi, \pi]$. Thus, substituting the endpoints of this interval into Eq. 3 and 6, we get: $\hat{v}_c \in [-2, 2]$ and $\hat{v}_f \in [-0.5, 0.5]$. Considering the maximum allowed carrier frequency error in a WLAN transceiver is ± 20 ppm according to the standard [7], this means that the maximum possible frequency error from the transmitter to the receiver is 40 ppm. For the 5 GHz band this means a maximum frequency error of around 200 KHz. With a subcarrier spacing of 312.5 KHz, this does not even exceed a single subcarrier spacing, which is well within the acquisition range of the coarse CFO estimation algorithm. Whether the acquisition range of the fine CFO estimation algorithm is met depends on the accuracy of the coarse algorithm since they are used sequentially. Thus, special attention should be paid to whether the estimation error of the coarse algorithm doesn't exceed this acquisition range.

2) Channel Estimation and Header Demodulation: After CFO synchronization using the preamble, the channel is estimated using the two LLTF sequences. Channel estimation is possible due to the receiver knowing the LLTF symbols and is performed according to Eq. 8. Here $\hat{H}_{k,\epsilon}$ is the complex channel estimate for each subcarrier k and lag ϵ, with respect to the perfect timing point. The channel estimate is the average estimate (denoted with $\langle\rangle$) over both LLTF symbols, where $Z_{LS_{n,k,\epsilon}}$ is the k^{th} subcarrier of the n^{th} received LLTF symbol with a lag ϵ with respect to the perfect timing point, and $a_{LS,k}$ is the k^{th} subcarrier of the transmitted LLTF symbol. Next, the frame header is demodulated and the header CRC is checked for errors.

$$\hat{H}_{k,\epsilon} = \langle \frac{Z_{LS_n,k,\epsilon}}{a_{LS,k}} \rangle \tag{8}$$

3) Joint SRO and Remaining CFO estimation: The next step in the receiver process is the combined operation of OFDM demodulation, joint SRO and CFO synchronization using OFDM symbol pilots and equalization of the fading channel. The joint SRO and CFO synchronization is a weighted least squares estimation algorithm based on [10], where any remaining CFO is estimated according to Eq. 9. This algorithm is further referred to as the remaining CFO estimation algorithm. In Eq. 9, k_j is the subcarrier index of the j^{th} pilot subcarrier, w_j is the weight for the j^{th} pilot subcarrier according to Eq. 11 and θ_j is the phase difference between the j^{th} pilot subcarriers symbols of the m^{th} OFDM symbol Z_{m,k_j} and its adjacent $(m-1^{\text{th}})$ OFDM symbol as described in Eq. 10. Finally, K is the length of an OFDM symbol, N_{cp} is the length of the cyclic prefix, and J is the total number of pilot subcarriers.

$$\hat{v}_r = \frac{\left(\sum_{j=0}^{J-1} w_j k_j^2\right)\left(\sum_{j=0}^{J-1} w_j \theta_j\right) - \left(\sum_{j=0}^{J-1} w_j k_j\right)\left(\sum_{j=0}^{J-1} w_j \theta_j k_j\right)}{(2\pi \frac{K+N_{cp}}{K})\left[\left(\sum_{j=0}^{J-1} w_j\right)\left(\sum_{j=0}^{J-1} w_j k_j^2\right) - \left(\sum_{j=0}^{J-1} w_j k_j\right)^2\right]} \tag{9}$$

with

$$\theta_j = \angle(Z_{m,k_j} Z^*_{m-1,k_j}) \tag{10}$$

and

$$w_j = |\tilde{H}_{k_j}|^2 = |\frac{Z_{m,k_j}}{a_{m,k_j}}|^2 \tag{11}$$

Note, $\hat{v}_r$ can be estimate for any adjacent pair of OFDM data symbols, e.g. for a system with 10 OFDM data symbols, 9 $\hat{v}_r$ estimates can be made. In this system it is assumed that the CFO remains constant throughout the frame, thus, the average of these estimates is used as the final $\hat{v}_r$ value. However, in a system where the CFO cannot be assumed to be constant, these 9 estimates can be used to track the remaining CFO as it changes throughout the frame.

4) SRO Compensation and Equalization: SRO on the received frames causes OFDM symbol window drift, i.e. symbol timing error increases throughout the received frame, causing Inter-Symbol Interference (ISI) as explained in [11]. Ideally, these errors are continuously evaluated, and when the timing error exceeds the one-sample threshold, the OFDM symbol window is corrected. An easier approach is forcing the symbol window to drift into the CP, this way no ISI occurs, only an integer timing offset is added to the symbols. As explained in [11], there are two cases: a positive SRO where the symbol window drifts towards the CP, and a negative SRO where the symbol window drifts away from the CP. For the second case (negative SRO), adding an initial integer timing offset towards the CP (i.e. a lag ϵ) means that for at least some time, the SRO will not cause ISI. This latter approach is chosen for this system with $\epsilon = 6$. The amount of OFDM symbols that will not be affected by ISI can be calculated using Eq. 12, where N_{sym} is the number of error free OFDM symbols, K is the length of an OFDM symbol, N_{cp} is the CP length of the OFDM symbols and ζ_{max} is the maximum negative SRO that can appear in the system expressed in ppm.

$$N_{\text{sym}} = \frac{\epsilon}{(K + N_{\text{cp}})\zeta_{\text{max}}} \tag{12}$$

For $\zeta = \pm 40$ ppm, $\epsilon = 6$, $K = 64$ and $N_{\text{cp}} = 16$, this comes to 1875 OFDM symbol. This is significantly higher than the maximum possible number of OFDM symbols in a WLAN frame, which is 1366.

However, adding this lag ϵ requires two things. First, the sign of the SRO should be known at the receiver. For the system at hand, this is satisfied because the SRO is fully known at the receiver. Secondly, the channel needs to be estimated using same lag, which will result in compensating the integer timing offset in the demodulated symbols when performing equalization. This is also the reason why the

OFDM demodulation, joint SRO and CFO synchronization and equalization operations are combined into one system block in Fig. 1, since their operations become intertwined as they all depend on ϵ.

Correcting for SRO and CFO, and performing equalization is done according to Eq. 13, where $\hat{a}_{m,k}$ are the estimated transmitted QAM data symbols and ζ is the SRO.

$$\hat{a}_{m,k} = Z_{m,k} \frac{1}{\hat{H}_{k,\epsilon}} e^{-i2\pi(1/K)(\hat{v}_r(1+\zeta)+k\zeta)(mK+N_{\text{cp}})} \quad (13)$$

5) Final Demodulation: Lastly, the receiver performs QAM demodulation, de-interleaving and decoding as the inverse operations of the transmitter, which results in the binary output.

III. Simulations & Analysis

Using the system model detailed in Section II, simulations were performed to analyze how well the CFO estimation algorithms (coarse, fine and remaining) perform when exposed to AWGN and CW EMI. This analysis looks at both average performance and worst case performance of the estimation algorithms in function of SIR and SNR and also in function of the CW interference frequency.

A. Simulations

To perform this analysis, simulations were performed with varying levels of E_b/N_0 (normalized Signal to Noise Ratio (SNR)) and Signal to Interference Ratio (SIR). For each combination of E_b/N_0 and SIR, 10^5 frames are generated with random AWGN (according to E_b/N_0) and a random CW interference where the CW amplitude depends on the SIR and the CW phase and frequency are random uniformly distributed variables according to Table I. Each frame is also affected by randomized synchronization errors: CPO φ, CFO v, FTO ϵ_f, ITO ϵ_I and SRO ζ, each random uniformly distributed values according to the values shown in Table I. In total there are 225 simulation points, consisting of all combinations of the 15 E_b/N_0 levels with the 15 SIR levels. Note that while the simulations were performed using E_b/N_0 values, the analysis uses SNR levels to facilitate a fair comparison with the various SIR levels. The relation between SNR and E_b/N_0 is shown in Eq. 14, where N_{bps} is the number of bits per OFDM symbol, R is the coderate and N_{sps} is the number of samples per OFDM symbol.

$$\text{SNR} = \frac{E_b}{N_0} + 10log_{10}(\frac{N_{\text{bps}}R}{N_{\text{sps}}}) \quad \text{[dB]} \quad (14)$$

Filling in the values $N_{\text{bps}} = 192$, $R = 1/2$ and $N_{\text{sps}} = 64 + 16$ according to Table I, the relation becomes:

$$\text{SNR} = \frac{E_b}{N_0} + 0.7918 \quad \text{[dB]} \quad (15)$$

TABLE I. Simulation Parameters

Parameter	value
Number of subcarriers: K	64
Cyclic prefix length	16
QAM order	16
Guard band carriers	left: 6, right: 5
DC carrier disabled	true
Pilot subcarriers indices	$-21, -7, 7, 21$
Coderate	1/2
Number of OFDM symbols per frame	10
Number of data subcarriers	48
Number of data bits per OFDM symbol	96
TGax Channel model delay profile	Model-B
Channel model environmental speed	0
Random carrier phase offset φ	$\varphi \sim U[0, 2\pi)$ radians
Random carrier frequency offset v	$v \sim U[-1.5, 1.5]$ subcarriers
Random integer timing offset ϵ_I	$\epsilon_I \sim U[0, 64] \in \mathbb{Z}$ samples
Random fractional timing offset ϵ_F	$\epsilon_F \sim U[0, 1)$ samples
Random sample rate offset ζ	$\zeta \sim U[-40, 40]$ ppm
CW amplitude A_{CW}	$A_{CW} = \sqrt{P_I} = \sqrt{\frac{Ps}{10^{SIR/10}}}$
CW Phase φ_{CW}	$\varphi_{CW} \sim U[0, 2\pi)$
CW Frequency f_{CW}	$f_{CW} \sim U[-32, 31)$
Number of frames per sim point	100000
Simulated E_b/N_0 levels	$\text{N} = \{-10, -5, 0, 5, ..., 60\}$ $\lvert\text{N}\rvert = 15$
Simulated SIR levels	$\text{I} = \{-10, -5, 0, 5, ..., 60\}$ $\lvert\text{I}\rvert = 15$
Number of sim points	$15 \cdot 15 = 225$

B. Estimation Errors

For each simulation point and for each CFO estimation algorithm, the mean absolute estimation error (MAE) and maximum absolute estimation error (MaxAE), expressed in a number of subcarriers spacings (or simply subcarriers), are calculated over the 10^5 simulated frames. The estimation errors for each algorithm for each frame are determined as follows:

$$\mathcal{E}_c = \nu - \hat{\nu}_c \quad (16)$$

$$\begin{aligned} \mathcal{E}_f &= \nu - \hat{\nu}_c - \hat{\nu}_f \\ &= \mathcal{E}_c - \hat{\nu}_f \end{aligned} \quad (17)$$

$$\begin{aligned} \mathcal{E}_r &= \nu - \hat{\nu}_c - \hat{\nu}_f - \hat{\nu}_r \\ &= \mathcal{E}_f - \hat{\nu}_r \end{aligned} \quad (18)$$

where $\mathcal{E}_c$, $\mathcal{E}_f$ and $\mathcal{E}_r$ are the estimation errors of the coarse, fine and remaining CFO estimation algorithms, respectively. Notice that $\mathcal{E}_f$ and $\mathcal{E}_r$ depend on the estimation error of the coarse and fine algorithm respectively. Since these algorithms are used sequentially in the receiver system, the error produced by one algorithm becomes the CFO that is input into the subsequent algorithm. As a consequence the final CFO estimation error of the system is $\mathcal{E}_r$.

C. Analysis and discussion

Figs. 5 and 6 show the mean and maximum absolute estimation errors for the CFO estimation algorithms in function of SIR (full lines) when no AWGN is present and SNR (striped lines) when no CW EMI is present. For ease of analysis, the estimation performance for a combination of a SNR and a SIR

value could be assumed to be the maximum of the selected points on each of the curves. For example when SNR $= 30$ dB then the MAE for the coarse algorithm is approximately 0.0005 and when SIR $= 10$ dB then the MAE for the coarse algorithm is approximately 0.03. Thus when SNR $= 30$ dB and SIR $= 10$ dB the MAE for the coarse algorithm can be assumed to be the error due to the CW EMI because it is highest.

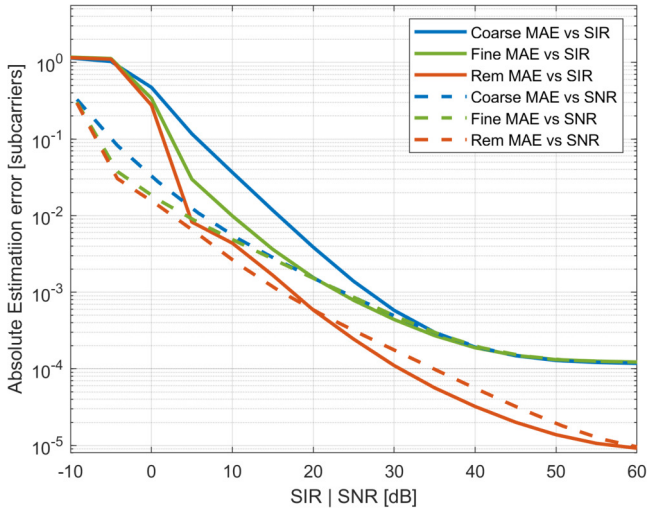

Fig. 5. Mean absolute estimation errors for coarse, fine and remaining frequency estimation algorithms vs SNR (when SIR$=60$ dB) and SIR (when SNR $= 60.7918$ dB).

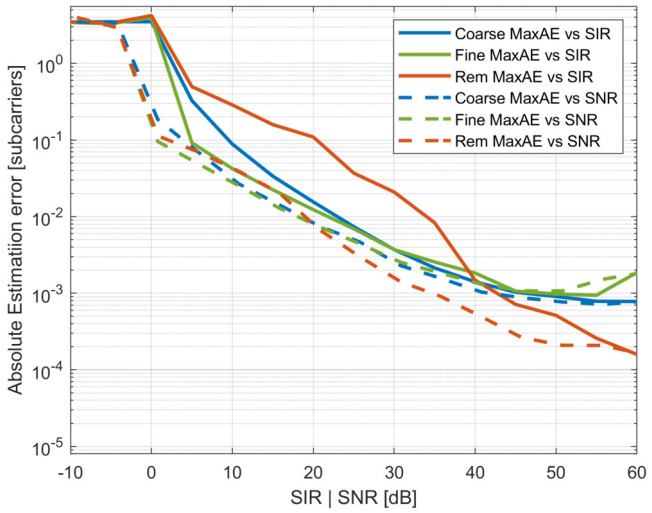

Fig. 6. Maximum absolute estimation errors for coarse, fine and remaining frequency estimation algorithms vs SNR (when SIR$=60$ dB) and SIR (when SNR $= 60.7918$ dB).

When observing the Mean Absolute Error (MAE) curves on Fig. 5, it can be seen that the average performance of the estimation algorithms becomes sequentially better, i.e. each algorithm from coarse, to fine, to remaining performs better (a lower MAE) than the previous. However, notice that the SNR and SIR curves for the same algorithm diverge at specific points. These divergence points are the points below which, for an equal amount of noise and EMI power, the CW EMI starts dominating the estimation performance. These points are roughly 30, 20 and 5 dB for the coarse, fine and remaining CFO estimation algorithms, respectively. This suggests that the remaining CFO algorithm is on average less sensitive to a CW EMI than the coarse and fine CFO estimation algorithms.

If a SNR level of around $25-30$ dB is assumed, which is a common operating point for high performance OFDM systems, the graphs in Fig. 5 show that all algorithms can already be dominated by a CW EMI with a SIR of 20 dB and below. Thus, under normal operating conditions, a CW EMI which is around 100 times less powerful than the signal power is already capable of noticeably influencing CFO estimation performance. Finally, since the estimation error of the remaining CFO estimation algorithm is the final estimation performance of the system, the system can be noticeably influenced by a CW EMI of 20 dB and below.

Looking at the MaxAE curves on Fig. 6 gives a different view. It can be seen that the algorithms don't perform sequentially better when exposed to CW EMI. In fact, the remaining algorithm under CW EMI exhibits significantly worse MaxAE performance than all other algorithms from around 38 dB SIR and below. From the MAE results in Fig. 5 alone, one might suggest that the system performs adequately in the presence of a CW EMI. However, taking into account the MaxAE errors reveals a significant risk of high estimation errors with the remaining CFO estimation algorithm. This suggests that the remaining algorithm might be suboptimal for URLLC systems where reliability is of utmost importance.

To understand this behaviour better, the mean estimation errors and MaxAE are plotted in function of the CW frequency in Figs. 7 and 8, respectively, for a SNR of 60.7918 dB and a SIR of 15 dB. Looking at these results, the mean estimation error of the coarse algorithm follows a cyclical pattern with a period of 4 subcarriers. This is no coincidence as the coarse algorithm uses the LSTF in the preamble for its algorithm, and this 4 subcarrier period corresponds perfectly to the frequency domain occupation of the LSTF, i.e. the LSTF in frequency domain only uses one in four of the OFDM system subcarriers. These results suggest that the CW frequency introduces an offset in the mean estimation error of the coarse CFO estimation algorithm depending on its distance to the nearest subcarriers. It is this frequency dependent offset that results the coarse estimation algorithm to have the highest MAE in function of SIR.

As for the fine and remaining mean estimation errors in function of CW frequency. The fine algorithm exhibits no noticeable frequency dependent behaviour, its estimation performance is constantly noisy across the whole frequency range. The remaining algorithm shows slight frequency dependant behaviour. It is noisy across the whole frequency range but the noise level varies from barely noticeable in most regions to very noticeable in four frequency bands, not surprisingly these bands are around the pilot subcarriers used for the algorithm.

Looking at the MaxAE curves in function of CW frequency in Fig. 8, it can be seen that the coarse and fine algorithms are relatively constant across the whole frequency range, with the coarse algorithm having slightly higher maximum absolute errors. On the other hand, the remaining algorithm shows four significant peaks in its maximum absolute errors. These four peaks again align with the four pilot subcarriers (-21, -7

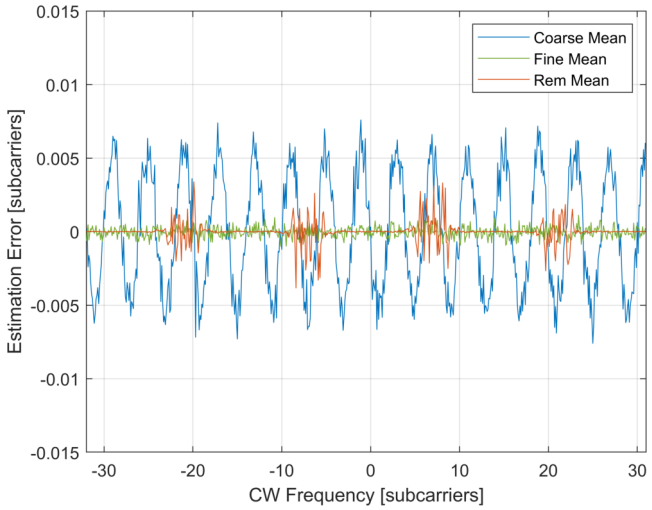

Fig. 7. Mean estimation errors for coarse, fine and remaining frequency estimation algorithms vs CW frequency for SNR= 60.7918 dB and SIR= 15 dB

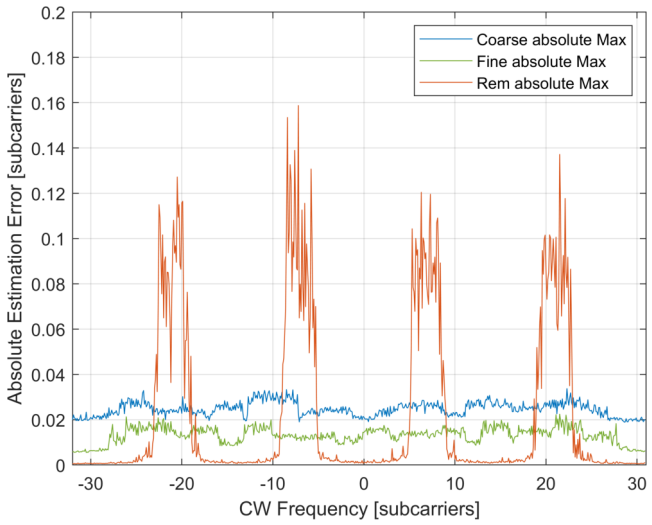

Fig. 8. Maximum absolute estimation errors for coarse, fine and remaining frequency estimation algorithms vs CW frequency for SNR= 60.7918 dB and SIR= 15 dB

,7 and 21), used in this algorithm, and they have a width of around 4 subcarriers, i.e. the peak around -7 stretches from subcarrier -9 to -5. More precisely, this indicates that the presence of the CW EMI in a two subcarrier distance from a pilot subcarrier has the potential to cause significant disruption to the performance of the remaining CFO estimation algorithm.

Intuitively this behaviour would not be expected. Instead it would be expected that the remaining algorithm estimation performance is only significantly influenced when the CW EMI frequency almost exactly aligns with one of the pilot subcarriers. However, this behaviour can be explained through the phenomena of spectral leakage. Since the remaining CFO estimation algorithm works in frequency domain, i.e. the algorithm uses the demodulated OFDM symbol pilots, the CW EMI is also subjected to this demodulation process, transforming it to the frequency domain using a Discrete Fourier Transformation (DFT). This frequency domain transformation causes spectral leakage of the CW EMI, smearing it out in frequency domain, when its frequency doesn't align closely with one of the discrete frequency bins. This is a well known phenomenon with narrowband signals and the DFT operation [12]. It is this smearing process that subjects the pilot subcarriers to the CW EMI even though its true frequency is two subcarriers away from the pilot.

This again leads to the conclusion that the use of the remaining CFO estimation algorithm in this state is inadvisable for URLLC systems. A potential solution for the high maximum estimation errors in the remaining CFO algorithm could be to disregard a pilot subcarrier affected by a CW EMI in the estimation algorithm. However, this would require a way to detect whether a pilot subcarrier is negatively affected by a CW EMI. This would also lower the estimation performance of the algorithm, although this can be combatted by adding more pilots into the system. Or better yet, since a CW EMI is a highly self-correlated signal, i.e. it is very predictable, we believe it is possible to remove its effect completely with negligible performance degradation for both the remaining CFO estimation algorithm and for the coarse and fine algorithms, by for example applying the algorithm from [13] to this problem.

IV. Conclusion and Future Work

A risk analysis was performed for Carrier Frequency Offset (CFO) estimation algorithms (coarse, fine and remaining) in a WLAN-based system under the influence of NBI, with a fully featured receiver. The WLAN-based system model was presented and the relevant synchronization algorithms were explained. This model was subsequently used to perform simulations for a range of SNR and SIR values with other simulation parameters being randomized.

From analyzing the simulation data, it was found that under normal operating conditions for a WLAN system, its CFO estimation algorithms can be noticeably affected by a NBI with a SIR of 20 dB and below. The analysis also identified divergence points for each algorithm, which is the point below which for an equal amount of interference and AWGN power, the NBI starts to dominate the estimation performance. These points are $30, 20$ and 5 dB for the coarse, fine and remaining CFO estimation algorithms, respectively. This shows that the remaining CFO estimation algorithm is, on average, the least sensitive to NBI. However, when analyzing the maximum absolute errors of each algorithm due to NBI, it was observed that the remaining CFO estimation algorithm performs significantly worse than the other algorithms. Further analysis showed that the maximum errors of the remaining CFO estimation algorithm become exceedingly large when the NBI is within a two subcarrier spacing distance of the used pilot subcarriers. Spectral leakage of the CW EMI due to it being subjected to the OFDM demodulation process is suspected to be the cause of this behaviour. For URLLC systems this maximum absolute error is by far more important than average performance as it influences system reliability the most. Therefore this problem should be investigated further.

Next steps in this work are as follows. First, analyze the respective contributions of the errors of each estimation algorithm to the system performance criteria, i.e. how much do these synchronization errors affect the Bit Error Rate (BER),

Packet Error Rate (PER) and Error Vector Magnitude (EVM) of the OFDM system. Second, perform a root-cause analysis, explaining why these algorithms are disturbed by NBI and what failure mechanisms are triggered. Third, designing CFO estimation algorithms which minimize the risk of CFO synchronization errors under NBI by, for example, minimizing the maximum absolute errors. Note the distinction between minimizing average performance and minimizing risk, the latter being crucial for URLLC systems. Lastly, the CW interference is the simplest NBI model, more complex/realistic NBIs could result in a substantially different effect on synchronization performance. Thus the effect of more complex and realistic NBIs on OFDM frequency synchronization algorithms should also be investigated.

REFERENCES

[1] G. Naik, B. Choudhury, and J.-M. Park, "IEEE 802.11bd & 5G NR V2X: Evolution of Radio Access Technologies for V2X Communications," *IEEE Access*, vol. 7, pp. 70 169–70 184, 2019.

[2] A. Coulson, "Bit error rate performance of OFDM in narrowband interference with excision filtering," *IEEE Transactions on Wireless Communications*, vol. 5, no. 9, pp. 2484–2492, 2006.

[3] B. Leeman, L. De Baets, S. Pollin, H. Hallez, D. Pissoort, and T. Claeys, "EM Risk Management for Wireless Communications: First Look and Case Study," in *2024 International Symposium on Electromagnetic Compatibility – EMC Europe*, 2024, pp. 296–301.

[4] M. Marey and H. Steendam, "The Effect of Narrowband Interference on Frequency Ambiguity Resolution for OFDM," in *IEEE Vehicular Technology Conference*, 2006, pp. 1–5.

[5] A. Coulson, "Narrowband interference in pilot symbol assisted OFDM systems," *IEEE Transactions on Wireless Communications*, vol. 3, no. 6, pp. 2277–2287, 2004.

[6] B. Leeman, H. Hallez, D. Pissoort, and T. Claeys, "Risk Analysis of Frequency Synchronization in WLAN-Based OFDM Systems Under Narrowband Interference," in *Proceedings of 2025 Joint European Conference on Networks and Communications & 6G Summit (EuCNC/6G Summit)*, June 2025, extended abstract.

[7] "IEEE Standard for Information Technology–Telecommunications and Information Exchange between Systems - Local and Metropolitan Area Networks–Specific Requirements - Part 11: Wireless LAN Medium Access Control (MAC) and Physical Layer (PHY) Specifications," *IEEE Std 802.11-2020 (Revision of IEEE Std 802.11-2016)*, pp. 1–4379, 2021.

[8] J. Liu, R. Porat *et al.*, "TGax Channel Model," September 2014, IEEE 802.11-14/0882r4.

[9] T. Schmidl and D. Cox, "Robust frequency and timing synchronization for ofdm," *IEEE Transactions on Communications*, vol. 45, no. 12, pp. 1613–1621, 1997.

[10] P.-Y. Tsai, H.-Y. Kang, and T.-D. Chiueh, "Joint weighted least-squares estimation of carrier-frequency offset and timing offset for OFDM systems over multipath fading channels," *IEEE Transactions on Vehicular Technology*, vol. 54, no. 1, pp. 211–223, 2005.

[11] M. Speth, S. Fechtel, G. Fock, and H. Meyr, "Optimum receiver design for wireless broad-band systems using OFDM. I," *IEEE Transactions on Communications*, vol. 47, no. 11, pp. 1668–1677, 1999.

[12] K. M. Fors, K. C. Wiklundh, and P. F. Stenumgaard, "On the Mismatch of Emission Requirements for CW Interference Against OFDM Systems," *IEEE Transactions on Electromagnetic Compatibility*, vol. 60, no. 5, pp. 1555–1561, 2018.

[13] A. Ovechkin, T. Claeys, D. Vanoost, G. A. E. Vandenbosch, and D. Pissoort, "A Novel Method of Removing the Influence of Continuous Electromagnetic Wave Disturbances in OFDM Systems," *IEEE Transactions on Electromagnetic Compatibility*, vol. 64, no. 2, pp. 338–347, 2022.